Spatial periodicities of defect environments in ^{57}Fe$_3$Al studied by Mössbauer powder diffractometry

Jiao Y. Y. Lin and Brent Fultz[*]

California Institute of Technology, Pasadena, California 91125, USA

Abstract. Mössbauer powder diffractometry was used to study partially-ordered ^{57}Fe$_3$Al. Multiple diffraction patterns were measured at Doppler velocities across all nuclear resonances in the sample. The superlattice diffractions were analyzed to provide data on the long-range order of Fe atoms having different numbers of Al neighbors. Comparing experimental data to calculations showed that Fe atoms having three Al atoms as first-nearest neighbors (1nn) have simple cubic long-range order, similar to that of Fe atoms with four Al 1nn. The simple cubic periodicity of Fe atoms with three Al 1nn was significantly lower than expected for homogeneous antisite disorder, however. Monte-Carlo simulations and transmission electron microscopy suggest that a significant fraction of aperiodic Fe atoms with three Al 1nn are near antiphase domain boundaries.

Introduction

Mössbauer diffractometry combines the capability of Mössbauer spectrometry to distinguish local chemical environments with the capability of diffractometry to measure long-range order (LRO) in materials. The spectrometry of hyperfine interactions, similar to that used in Mössbauer spectrometry, can emphasize scattering from ^{57}Fe atoms in specific chemical environments. With this chemical selectivity, the spatial periodicities of ^{57}Fe atoms in different chemical environments can be determined from the energy-dependence of the nuclear Bragg diffractions. The measurements are enabled by developments in both the theory and practice of Mössbauer powder diffractometry, many of which occurred in the past decade [1–10].

At high temperatures, Fe$_3$Al has the bcc structure, and develops simple cubic (sc) order with the B2 structure at temperatures below 800 °C. Below 550 °C the equilibrium structure is the D0$_3$ structure, where Al atoms occupy one of four face-centered cubic (fcc) sublattices of the D0$_3$ structure (we denote this Al-rich sublattice as δ). By rapid quenching, Fe$_3$Al can be prepared as a non-equilibrium, disordered solid solution. Subsequent annealing at low temperatures produces a number of peculiarities, such as the formation of the B32 structure, which may be a kinetic transient [11–13], or perhaps driven by magnetic interactions in sub-stoichiometric zones [14]. During annealing, conventional Mössbauer spectrometry is capable of measuring the defect environments in partially ordered Fe$_3$Al. It can quantify the fractions of Fe atoms with different numbers of Al first-nearest neighbors [15–17]. Iron atoms in these defect environments may have spatial periodicities, however, perhaps like Fe atoms in the B2, B32, or D0$_3$ structures.

The first direct measurements of spatial periodicities of defect environments in a material were performed recently [10]. Mössbauer diffraction patterns were measured over the full Mössbauer energy spectrum of an alloy of ^{57}Fe$_3$Al, making it possible to quantify the unknown spatial periodicity of ^{57}Fe atoms with (3) and (5) Al 1nn atoms. [The notation "(n) Al 1nn" denotes a chemical environment where a ^{57}Fe atom has n Al atoms as first-nearest-neighbors.] It was found that the Fe atoms in these defect environments have some sc periodicity. The data were further analyzed to obtain the occupancies of the four sublattices of the D0$_3$ structure, with no assumptions that would select B2 over B32 chemical order. No evidence for B32 order was found for any chemical environments.

The prior analysis of these data [10] showed a significant discrepancy between the measured and calculated simple-cubic long-range order parameter for ^{57}Fe atoms in the (3) Al 1nn environment. With further Monte-Carlo simulations and transmission electron microscopy study of the alloy structure, explored in the present work, it was possible to show that the discrepancy between the calculated and measured chemical environments likely originates with a non-random point defect population at antiphase domain boundaries in the crystals.

Materials and experimental procedures

The sample of ^{57}Fe$_3$Al was prepared from ^{57}Fe of 95% isotopic enrichment and 99.99% chemical purity, and Al metal of 99.999% chemical purity. These metals were processed by arc-melting, splat-quenching and cold-rolling,
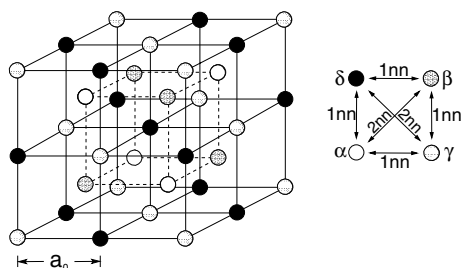
---

[*] Correspondence author (e-mail: btf@caltech.edu)

followed by an annealing for 100 h at 450 °C to develop $D0_3$ chemical order [7]. Conventional X-ray powder diffractometry was used to confirm a high degree of $D0_3$ LRO in the sample. For the transmission electron microscopy (TEM) measurements, a new sample of Fe_3Al was prepared following the heat treatment schedule used for the sample of $^{57}Fe_3Al$. (The sample was not given an initial cold-rolling, however.) Disks of 3 mm diameter were punched from the foil, and thinned to electron transparency by twin-jet electropolishing. The electrolyte was 20% perchloric acid in 80% methanol, cooled to −35 °C.

The Mössbauer powder diffractometer consisted of a Bruker X-1000 Xe-filled area detector, a GE XRD-5 goniometer, a ^{57}Co (Rh) radioactive source, a Wissel Doppler drive system with laser interferometer velocity calibrator, and a control computer. This instrument was described recently [8, 10, 18]. All Mössbauer diffraction patterns were normalized to incident flux, with units of counts/sr/(mCi · hour).

In iron alloys containing up to nearly 30% aluminum, conventional Mössbauer energy spectra comprise sets of partially-overlapping sextets of absorption peaks. To a good approximation, each sextet has the same pattern of splitting, but a unique width for its splitting, depending on the number, n, of Al atoms in the 1nn shell of the ^{57}Fe atom [13]. The amount of splitting is directly proportional to the hyperfine magnetic field at the ^{57}Fe atom, as is well known. For Fe–Al alloys, the HMF for Fe with (0) Al 1nn is approximately 310 kG, and that of Fe with (4) Al 1nn is approximately 215 kG. A perfect $D0_3$ structure has two types of 1nn environments for Fe atoms – two-thirds of the Fe atoms have (4) Al 1nn atoms, and the other one-third have (0) Al 1nn atoms. Figure 1 shows that these latter Fe atoms are arranged as an fcc structure with a unit cell edge of twice the edge length of the bcc cube (γ sublattice). Note also from Fig. 1 that the Fe atoms having a (4) Al 1nn environment are arranged as a simple cubic (sc) structure. Experimental confirmation of this structural fact was published previously when Mössbauer diffraction patterns were measured by tuning the incident photons to nuclear resonances of ^{57}Fe atoms in (0) and (4) Al 1nn environments [5].

Other first-nearest-neighbor chemical environments exist for ^{57}Fe in an Fe_3Al alloy with imperfect chemical order. These occur with other values of HMF. In our sample, the most prominent defect environment for ^{57}Fe is the

(3) Al 1nn environment, for which the HMF is approximately 255 kG. The (3) Al 1nn environment is a defect environment. It is characteristic of neither the $D0_3$ nor the B2 structures.
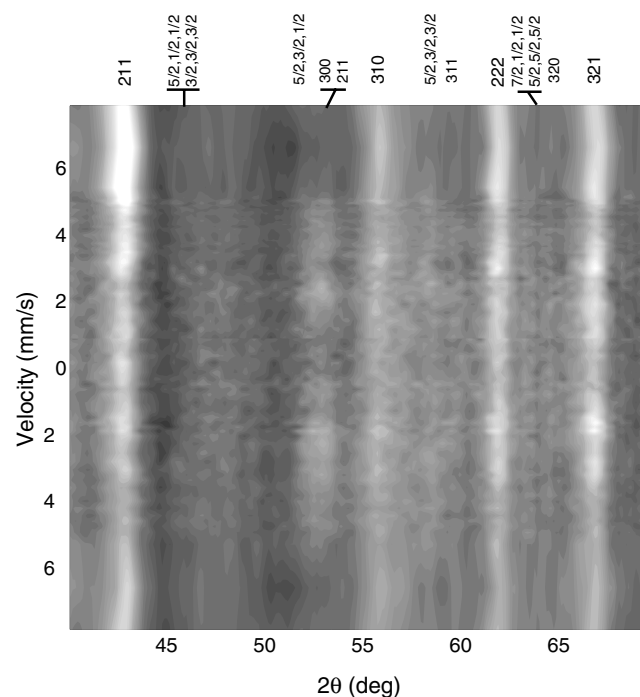
Measured Mössbauer diffraction intensities

Intensities of fundamental bcc diffractions

Mössbauer diffraction intensities are presented in Fig. 2. The intensities of the fundamental diffraction peaks are

$$I = \left| F^{Al}(\varepsilon)\, c^{Al} + \sum_{n=0}^{8} F^{(n)}(\varepsilon)\, c^{(n)} \right|^2 , \qquad (1)$$

where $F^{Al}(\varepsilon)$ and $F^{(n)}(\varepsilon)$ denote the scattering factors for Al atoms and Fe atoms with (n) Al 1nn, respectively, and vary with the Doppler shift energy, ε. The intensities of the fundamental diffraction peaks do not depend on the long-range chemical order (LRO) on the bcc lattice, but they do depend on the short-range order (SRO) of the local chemical environments of ^{57}Fe because the energy spectrum (intensity versus ε) of the nuclear scattering amplitude, $F^{(n)}(\varepsilon)$, depends on SRO. Expressions for the form factor for nuclear resonant scattering, including polarization effects, $F^{(n)}(\varepsilon)$, were given previously [10]. Analysis of the energy spectra of the bcc fundamental diffractions gave probabilities for ^{57}Fe atoms having different numbers, n, of Al atoms in their 1nn shells (see Table 1). A similar analysis was performed on a conventional conversion electron Mössbauer spectrum (CEMS) from the sample.

Fig. 1. The $D0_3$ structure and its four fcc sublattice with lattice parameter equal to $2a_0$. For Fe_3Al, Al atoms occupy the δ sublattice, while Fe atoms occupy the other three fcc sublattices. Fe atoms in α and β sublattices have 4 Fe 1nn atoms and 4 Al 1nn atoms, while Fe atoms in γ sublattice have 8 Fe 1nn atoms. Note that the combination of α and β sublattices forms a sc structure with lattice parameter a_0.

Fig. 2. Mössbauer diffraction patterns from $^{57}Fe_3Al$, taken at 89 velocities arranged vertically. Data were normalized by incident flux, and background was subtracted. Range for each pixel is from −200 counts (black) to +850 counts (white).

Table 1. First-nearest-neighbor chemical environments in partially-ordered Fe_3Al.

	(0,1) Al	(2) Al	(3) Al	(4) Al	(5) Al
CEMS spectra	0.290	0.116	0.138	0.388	0.025
Mössbauer diffraction spectra	0.248	0.132	0.110	0.373	0.083

Order parameters and superlattice diffractions

For the $D0_3$ structure there are two types of superlattice diffractions: (100)-type for sc periodicities and $(^1/_2\,^1/_2\,^1/_2)$-type for fcc periodicities. The scattering factors for these diffractions include a phase factor for each of the four fcc sublattices of the $D0_3$ structure as listed in Table 2. For Mössbauer diffraction we define order parameters for each chemical environment (n) in terms of the concentration of the chemical environment on each sublattice. For example the concentration of a chemical environment (n) on the α sublattice is $c_\alpha^{(n)}$. The two types of LRO parameters are

$$\eta_{sc}^{(n)} = \frac{c_\alpha^{(n)} + c_\beta^{(n)} - c_\gamma^{(n)} - c_\delta^{(n)}}{c^{(n)}} \ , \qquad (2)$$

and

$$\eta_{fcc}^{(n)} = \frac{c_\alpha^{(n)} - c_\beta^{(n)} + i\,(c_\gamma^{(n)} - c_\delta^{(n)})}{c^{(n)}} \ . \qquad (3)$$

The quantity $\eta_{sc}^{(n)}$ is a measure of the B2 order between two sc sublattices ($\delta + \gamma$ vs. $\alpha + \beta$), while the real and imaginary parts of $\eta_{fcc}^{(n)}$ are measures of order between two pairs of fcc sublattices (δ vs. γ and α vs. β). Parameters $\eta_{sc}^{(n)}$ and $\eta_{fcc}^{(n)}$ combined with the total concentration $c^{(n)}$ give all information about the sublattice occupancy of the chemical environment (or atomic species), (n), $\{c_\alpha^{(n)}, c_\beta^{(n)}, c_\gamma^{(n)}, c_\delta^{(n)}\}$, from which the diffraction intensities can be calculated [10].

Simple cubic periodicities

Using the HMF distribution obtained from fundamental diffraction peaks, the superlattice diffraction energy spectra were fitted using $\eta_{sc}^{(n)}$ and $\eta_{fcc}^{(n)}$ as adjustable parameters [10].

Figure 3 presents the experimental data and calculated energy spectra of superlattice diffraction peaks (300) and $(^5/_2\,^3/_2\,^3/_2)$. Order parameters providing the best fit are listed in Table 3. The error bars were estimated from the covariance matrix. To show the sensitivity of the diffraction energy spectra to the order parameters $\eta_{sc}^{(n)}$, various simulated energy spectra of superlattice diffractions are presented in Fig. 4. The energy spectrum of the (300) diffraction is very sensitive to the B2 order of Fe atoms with

Table 2. Phase factors for the four fcc sublattices in the $D0_3$ structure for (100)-type and $(^1/_2\,^1/_2\,^1/_2)$-type diffractions.

	α	γ	β	δ
(100)	1	−1	1	−1
$(^1/_2\,^1/_2\,^1/_2)$	1	i	−1	−i
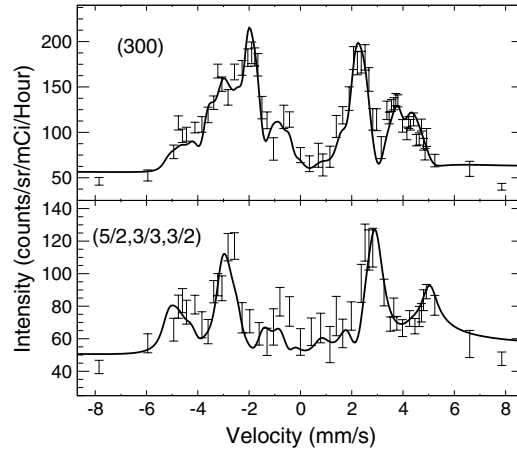
Fig. 3. Full energy spectra of (300) and $(^5/_2\,^3/_2\,^3/_2)$ diffraction intensities from Fe_3Al, including kinematical theory calculations and experimental data.
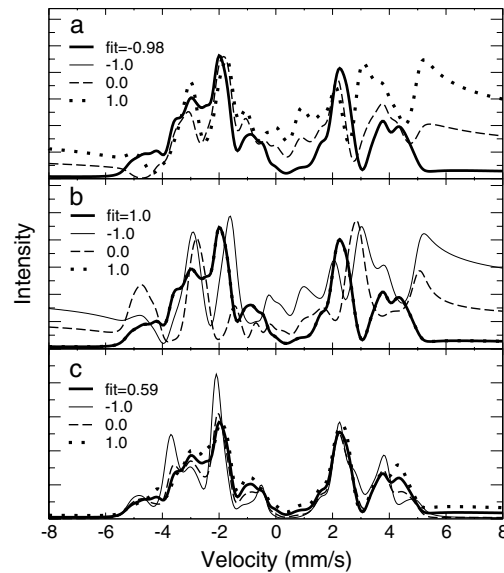
Fig. 4. Sensitivity of simulated energy spectra of (300) diffraction peak to variations of LRO parameter $\eta_{sc}^{(n)}$ for (**a**) Fe atoms with (0) Al $1nn$, (**b**) Fe atoms with (4) Al $1nn$, and (**c**) Fe atoms with (3) Al $1nn$. The thick lines are the best fit to experimental data with $\eta_{sc}^{(0)} = -0.98$, $\eta_{sc}^{(4)} = 1.0$ and $\eta_{sc}^{(3)} = 0.59$. Some lines are invisible due to overlap with curves of the best fit: the thin line with $\eta_{sc}^{(0)} = -1.0$ in (a), and the dotted line with $\eta_{sc}^{(4)} = 1.0$ in (b).

(0) or (4) Al $1nn$. From these fits, we find that the (0) and (4) Al $1nn$ environments have B2 order parameters of nearly 1.0. The (3) Al chemical environments have a B2 order of $\eta_{sc}^{(3)} = 0.6$.

Monte-Carlo simulations of diffraction intensities

Simulations of alloys and diffractions

A set of bcc alloys with two atom types in a 3 : 1 ratio were constructed on a computer, usually in states of chemical disorder. A vacancy mechanism of diffusion was implemented with a Monte-Carlo algorithm that allowed a vacancy to exchange sites with atoms in its $1nn$ shell [19–20]. The exchange probability was set by activated-state rate theory, being less probable for atoms having an energetically-fa-

Table 3. Measured LRO Parameters for prominent chemical environments of Fe and Al.

^{57}Fe environment	$\eta_{\text{sc}}^{(n)}$	Im $[\eta_{\text{fcc}}^{(n)}]$	Re $[\eta_{\text{fcc}}^{(n)}]$	$c^{(n)}$
(0) Al 1nn	-0.98 ± 0.01	0.98 ± 0.25	-0.00 ± 0.31	0.16 ± 0.01
(1) Al 1nn	-0.81 ± 0.45	0.51 ± 0.80	-0.09 ± 0.70	0.03 ± 0.01
(2) Al 1nn	-0.35 ± 0.13	0.61 ± 0.45	-0.29 ± 0.55	0.10 ± 0.01
(3) Al 1nn	0.59 ± 0.05	-0.20 ± 0.45	-0.18 ± 0.44	0.09 ± 0.01
(4) Al 1nn	1.00 ± 0.01	0.00 ± 0.01	0.02 ± 0.27	0.28 ± 0.01
(5) Al 1nn	0.87 ± 0.10	-0.07 ± 0.70	0.93 ± 1.18	0.06 ± 0.01
Al atom	-0.70 ± 0.20	-0.80 ± 0.30	-0.01 ± 0.35	0.25

vorable set of neighbors. Various choices of chemical interactions between 1nn and 2nn pairs of atoms were used in the simulations. The simulations were stopped when the alloy possessed the 1nn chemical environments of Table 1, and had a high degree of D0$_3$ LRO, consistent with the conventional X-ray diffraction pattern.

Within each simulated alloy, we identified all Fe atoms having different numbers of 1nn Al atoms. For example, we found the coordinates, $\{\vec{r}_3\}$, of all Fe atoms with the (3) Al 1nn environment. We set the scattering factor of these Fe atoms to 1, all others to zero, and calculated the scattered wave

$$\psi_3(\Delta\vec{k}) = \sum_{\vec{r}_3} e^{i\,\Delta\vec{k}\cdot\vec{r}_3} \ . \tag{4}$$

We obtained the diffracted intensity from the Fe atoms with this (3) Al 1nn environment as $I_3(\Delta\vec{k}) = |\psi_3(\Delta\vec{k})|^2$. The same procedure was used for the diffracted intensities of other chemical environments, the (0) and (4) Al 1nn environments, I_0 and I_4, for example. As expected from the arrangements of these two Fe sites in Fig. 1, the intensity I_0 showed a family of $(^1/_2\,^1/_2\,^1/_2)$ diffraction peaks plus the (100) family, whereas I_4 showed only the (100) family. Interestingly, the calculated intensity I_3 showed the (100) family of diffractions, and their intensities were strong. For example, the simulated intensity of Eq. (7), normalized to the number of Fe atoms having the (3) Al 1nn environment, was much larger than the B2 LRO parameter of 0.59 found for Fe atoms in the (3) Al 1nn environment (Table 3). Simulations were performed with a range of ratios for 1nn and 2nn interatomic interactions that produce D0$_3$ chemical order, and these potentials provided an average of 0.94 for $\eta_{\text{sc}}^{(3)}$. The discrepancy between 0.59 and 0.94 is well outside the experimental error.

A second type of computer simulation was performed to generate "homogeneous disorder". The simulation began with a structure having perfect D0$_3$ order. Random interchanges of Al atoms off the δ-sublattice were then performed until each Al atom was swapped for an Fe atom.

The (3) Al 1nn defect environment

Homogeneous disorder

The chemical environment of Fe atoms with (3) Al 1nn is a defect environment, so its large B2 LRO parameter may seem surprising. Defect environments, originating with antisite atoms on a D0$_3$ sublattice, are expected to have some periodicity, however. The simplest creation of anti-

site defects is by randomly exchanging atoms in an initially-ordered D0$_3$ structure, a model we term "homogeneous disorder". For homogeneous disorder, when an antisite Fe atom is on the δ-sublattice, its neighboring Fe atoms with (4) Al 1nn will be transformed to Fe atoms with (3) Al 1nn. The transformation is efficient because one antisite Fe atom can produce 8 Fe atoms with (3) Al 1nn, if no other antisite defects are nearby. At low concentrations, these Fe atoms with (3) Al 1nn have exactly the same LRO as Fe atoms with (4) Al 1nn. For a D0$_3$-ordered domain with few defect atoms, the B2 LRO parameter for Fe atoms with (3) Al 1nn is, therefore, $\eta_{\text{sc}}^{(3)} \simeq 1$.

The SRO and LRO parameters for different amounts of homogeneous disorder were obtained from simulations, and are presented in Figs. 5 and 6. Figure 5 shows that for the near-perfect D0$_3$ structure (near 0% antisite defects), the Fe atoms have primarily 0 and 4 Al atoms in their 1nn shells. The fractions of these environments decrease with increasing numbers of antisite defects. The state of full disorder, a random solid solution of Fe-25 at.% Al, exists when the antisite defect concentration is 0.75 (beyond this there is some D0$_3$ order with Fe atoms on the Al sublattice). At the antisite defect concentration of 0.75, the probabilities for Fe atoms having n Al neighbors are equal to the binomial probability, $p(8, n, 0.25) = \{8!\,[(8-n)!\,n!]^{-1}\}\,0.25^n\,0.75^{(1-n)}$. At this antisite defect concentration of 0.75, all LRO parameters are zero.

It is straightforward to test if the experimental measurements are consistent with the homogeneous disorder of Figs. 5 and 6. With an experimental SRO of approximately 0.13 for the (3) Al 1nn chemical environments, Fig. 5 shows that the concentration of antisite defects is approximately 0.07. Figure 6 shows that for an antisite defect of 0.07, the
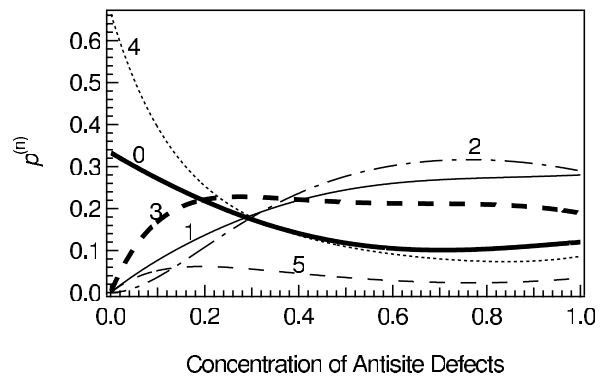
Fig. 5. Short-range order with random antisite defects, obtained from simulations of homogeneous disorder. The axis $p(n)$ is the fraction of ^{57}Fe atoms having the number n Al atoms in their 1nn shell. Labels denote numbers, (n), of Al 1nn atoms about ^{57}Fe atoms.
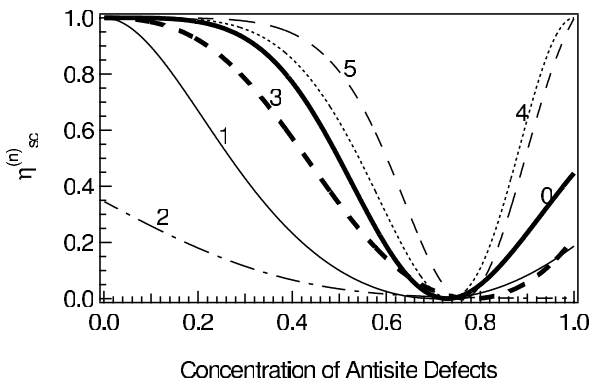
Fig. 6. Long-range order with random antisite defects, obtained from simulations of homogeneous disorder. The LRO parameter, η_{sc}, was obtained from Eq. 4 as explained in text. Labels denote numbers, (n), of Al $1nn$ atoms about ^{57}Fe atoms.

(3) Al $1nn$ chemical environments have a high B2 LRO parameter, nearly 1.0. Figures 5 and 6, based on a homogeneous random distribution of antisite atoms, predict that the B2 LRO of (3) Al $1nn$ chemical environments should be much higher than our experimental results.

Effects of antiphase boundaries

We seek to understand why the LRO of (3) Al $1nn$ environments measured by Mössbauer diffractometry is 0.59, rather than nearly 1.0. One possibility is suggested by a Monte-Carlo simulation of ordering kinetics presented in Fig. 7. This figure shows that the LRO of (3) Al $1nn$ chemical environments undergoes a sharp increase at Monte-Carlo step number 10,000, well after the (0) and (4) Al $1nn$ environments have developed order. Graphical displays of the atom arrangements at this late stage of the simulation showed the disappearance of the antiphase boundaries. It therefore seems that the (3) Al $1nn$ chemical environments in the neighborhood of an antiphase boundary have smaller LRO than those in other regions.

Since the four variants of the D0$_3$ structure are determined by the position of the Al sublattice, an antiphase boundary (APB) can be characterized by the displacement of the Al sublattices across the APB. Antiphase boundaries are either B2-type, for which the displacement vector is $a_0\langle^1\!/_2\,^1\!/_2\,^1\!/_2\rangle$, or D0$_3$-type, for which it is $a_0\langle100\rangle$ [21]. The plane of the APB is also specified, e.g., (hkl).
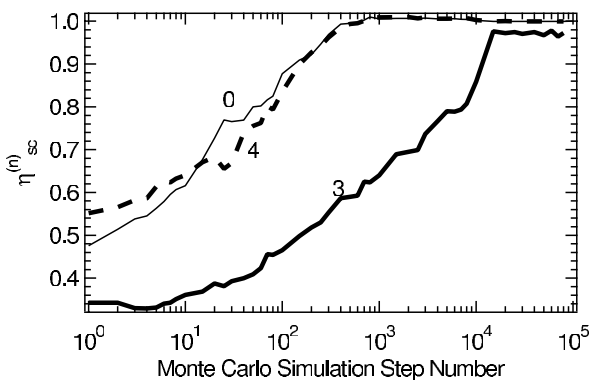
Fig. 7. Development of B2 LRO of the different Al neighborhoods of ^{57}Fe, calculated by Monte-Carlo simulation. Labels denote numbers, (n), of Al $1nn$ atoms about ^{57}Fe atoms.
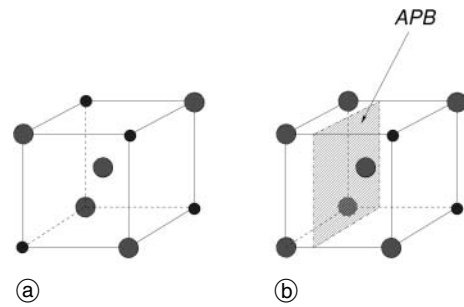
Fig. 8. Geometry of a B2-type APB on a (100) plane. The Fe atoms are represented by bigger spheres and Al atoms are smaller. (**a**) A structure without APB. The Fe atom at the center has 4 Al and 4 Fe $1nns$. (**b**) A B2-type APB is inserted between the central Fe atom and the 4 atoms on the left.

An APB alters chemical environments by shifting pairs of atoms across the boundary. Only atoms in pairs whose bonds are cut by the APB can have changes to their chemical environments. A D0$_3$-type APB changes only $2nn$ bonds [21]. Second neighbors cause only weak effects on the ^{57}Fe hyperfine magnetic field, so we can neglect D0$_3$-type APBs. We concern ourselves only with B2-type APBs, an example of which is presented in Fig. 8. The central Fe atom in Fig. 8a has 4 Al and 4 Fe atom neighbors. The B2-type APB on the (100) plane in Fig. 8b brings four Fe atoms to the left of the APB (these four Fe atoms were originally on the α and β sublattices). This particular APB transforms a (4) Al $1nn$ chemical environment to a (2) Al $1nn$ chemical environment. Similarly, an Fe atom having a (0) Al $1nn$ environment will also be transformed to a (2) Al $1nn$ environment. (These facts were confirmed by computer constructions of several B2-type APBs.) Similar analysis and computer constructions of B2-type APBs on (111) and (110) planes showed the formation of (1) and (3) Al $1nn$ chemical environments on the boundary. None of these Fe atoms had fcc or sc spatial periodicities. With further thought one concludes that B2-type APBs on planes other than (100), (110) and (111) will induce combinations of (1), (2) and (3) Al $1nn$ chemical environments.

In summary, B2-type APBs can produce Fe atoms with (1), (2) or (3) Al $1nn$ environments, depending on the orientation of the boundary. The Fe atoms whose bonds are modified by the APB could be on any sublattice except the Al sublattice. These defect environments are almost evenly distributed over all four fcc sublattices, and have neither fcc-type nor sc-type LRO.

We understand the LRO parameter $\eta_{sc}^{(3)} \simeq 0.6$ for (3) Al $1nn$ environments as follows. For homogeneous disorder of a few random antisite defects, the Fe atoms with (3) Al $1nn$ are highly ordered. On the other hand, an antiphase boundary produces (3) Al $1nn$ chemical environments on all sublattices. Together these two mechanisms can produce various states of LRO for (3) Al $1nn$ chemical environments, with order parameters $\eta_{sc}^{(3)}$ ranging from 0 to 1.

The APBs are responsible for a fraction of iron atoms having the (3) Al $1nn$ environment, f_3^{APB}:

$$f_3^{APB} = \overline{\left(\frac{6a_0}{l\,0.75}\,\kappa\right)} = 8\kappa a_0 \overline{l^{-1}}, \tag{5}$$
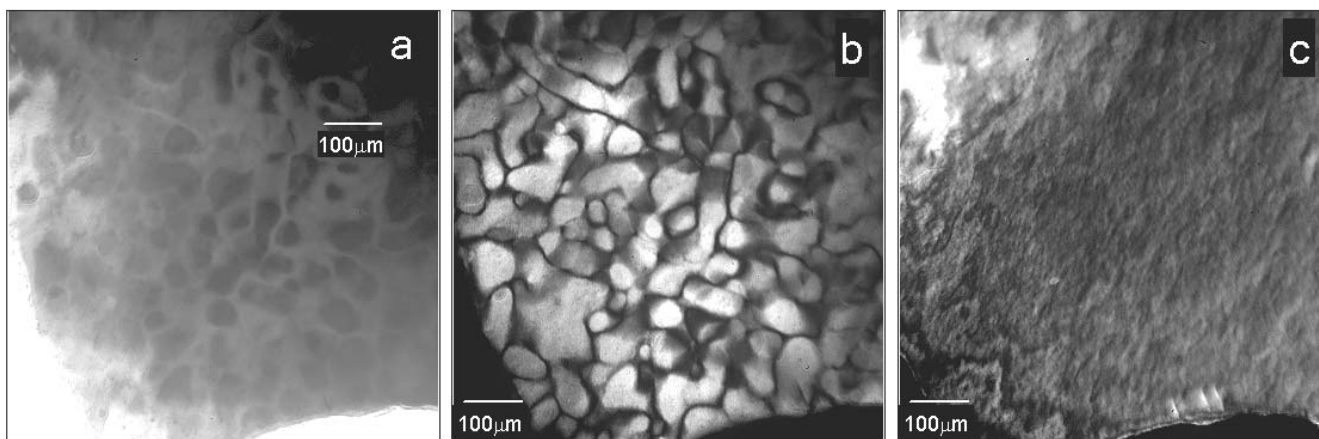
Fig. 9. TEM images of B2-type APBs in ordered Fe3Al: (**a**) bright-field image, (**b**) axial dark-field image using a (100) superlattice diffraction, (**c**) axial dark-field image using a (200) diffraction.

where the factor of 6 is an approximation to scale the number of atom sites at the domain boundary to the number of sites in the domains (a cubical domain has 6 surfaces). The factor 0.75 is the fraction of all atoms that are Fe. The lattice constant is a_0, and is 0.289 nm. The domain size is l, and $\overline{l^{-1}}$ is the averaged inverse-domain-size. The fraction of (110) and (111)-direction APBs in all APBs is κ, which is expected to be on the order of 0.5[1], because there is no preference in the directions of APBs [21].

From Table 1, the fraction of all Fe atoms having the (3) Al $1nn$ chemical environments is 0.14, so the homogeneous disorder is responsible for a fraction of iron atoms having the (3) Al $1nn$ environment equal to $f_3^{HD} = 0.14 - f_3^{APB}$. The total B2 LRO of 0.6 can be estimated as $0.6 = [(0.14 - f_3^{APB}) \times 0.9 + f_3^{APB} \times 0.0]/0.14$, which provides $f_3^{APB} = 0.05$, and hence a fraction $f_3^{HD} = 0.09$ from homogeneous disorder. Substituting this f_3^{APB} into Eq. 5 provides $\overline{l^{-1}} = [23 \text{ nm}]^{-1}$. This is close to what we estimate from the broadenings of the superlattice X-ray diffractions, although these measurements are not so accurate for domains of this size.

Transmission electron microscopy study of antiphase domain boundaries

The dark-field imaging technique of transmission electron microscopy is especially well-suited for determining the sizes of domains in ordered alloys. The interest here is in identifying the sizes of B2-type domains, since these are capable of producing aperiodic defect environments for Fe atoms with (3) Al $1nn$.

Figure 9 shows a bright-field image and two dark field images, taken with a superlattice (100) diffraction and a fundamental (200) diffraction. The diffraction conditions used for these images are shown in Fig. 10. It is significant that the rounded dark lines are visible for the (100) dark-field image, but not for the (200) dark-field image.
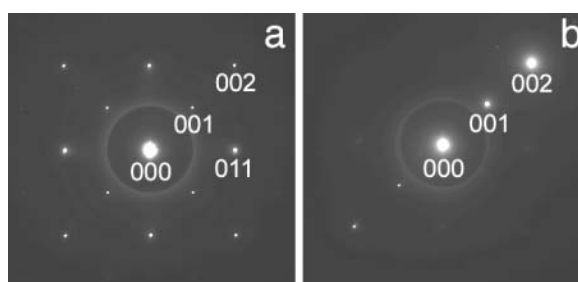
Fig. 10. Diffraction patterns showing the conditions used for the bright-field and dark-field images of Fig. 9. (**a**) (100) zone axis used, (**b**) actual tilt used for imaging.

This shows that the curved lines in Fig. 9b are from antiphase domain boundaries [21]. Some domain boundary contrast is expected in the bright field image, owing to the modest intensity of the (001) diffraction in Fig. 10b. The average size of the domains was determined by drawing lines at random through the image of Fig. 9b, and collecting a histogram of line segments between boundaries. Assuming the sample to be thin compared to the size of the domains, the average length of a line segment is properly volume-averaged for use as $\overline{l^{-1}}$ in Eq. 5. From images such as Fig. 9b we obtained $\overline{l^{-1}} = [46 \text{ nm}]^{-1}$. This is of the right order, but approximately half as large as needed to account for all aperiodic Fe atoms having the (3) Al $1nn$ environment. This suggests the presence of other sources of disordered Fe environments, but there are uncertainties from the approximations in our analysis, and perhaps differences in the samples.

Conclusions

A Mössbauer powder diffractometer was used to measure energy spectra of the nuclear and electronic Bragg diffractions from a partially-ordered sample of $^{57}Fe_3Al$. Analysis of the data showed, for example, that Fe atoms with (0) and (4) Al $1nn$ environments have the expected spatial LRO of the D0$_3$ structure. More importantly, the present research provided information on the periodicity of defect environments of Fe atoms, i.e., the periodicities of Fe atoms having three Al atoms in their first-nearest-neighbor shell.

---

[1] This is a conservative estimate. Actually, there are 6 kinds of (100) planes, but 12 of (110) and 8 of (111). If these are the only planes, and exist with equal probabilities, then $\kappa = \frac{20}{26}$.

It was found that Fe atoms with the (3) Al 1*nn* environment have a sc LRO parameter of 0.6. Some Fe atoms in the (3) Al 1*nn* environment are probably neighbors of antisite Fe atoms on the δ sites of the D0$_3$ structure (the Al-rich sublattice is denoted δ). A random distribution of Fe atoms on the δ-sublattice provides a large sc order parameter of nearly 1.0, however. Antiphase domain boundaries are another source of Fe atoms with the (3) Al 1*nn* environment, and simulations indicate that these Fe atoms have no LRO. A mix of Fe atoms adjacent to APBs, plus other Fe atoms distributed on the δ-sublattice, can account for the measured periodicity of the Fe atoms in the (3) Al 1*nn* environment. Transmission electron microscopy measurements of domain size indicate that this source of disorder at APBs is important, but additional sources are possible.

References

[1] O'Conner, D. A.; Black, P. J.: Theory of nuclear resonant and electronic scattering of resonant radiation by crystals. Proc. Phys. Soc. **83** (1964) 941–948.

[2] Belyakov, V. A.: Crystal diffraction of Mössbauer gamma-radiation. Usp. Fiz. Nauk 115: 553–601, English translation: Sov. Phys. Usp. **18** (1975) 267–291.

[3] Tegze, M.; Faigel, G.: Mössbauer diffraction measurements on polycrystalline bcc iron. Hyperfine Interact. **92** (1994) 1137–1141.

[4] Stephens, T. A.; Keune, W.; Fultz, B.: Mössbauer-effect diffraction from polycrystalline ^{57}Fe. Hyperfine Interact. **92** (1994) 1095–1100.

[5] Stephens, T. A.; Fultz, B.: Chemical environment selectivity in Mössbauer diffraction from ^{57}Fe$_3$Al. Phys. Rev. Lett. **78** (1997) 366–369.

[6] Fultz, B.; Stephens, T. A.: Mössbauer diffraction and interference studies of polycrystalline metals and alloys. Hyperfine Interact. **113** (1998) 199–217.

[7] Stephens, T. A.: Chemical environment selectivity in Mössbauer Diffraction. PhD thesis, California Institute of Technology, 1996.

[8] Kriplani, U.; Lin, J. Y. Y.; Regehr, M.W.; Fultz, B.: Intensities of Mössbauer diffractions from polycrystalline bcc ^{57}Fe. Phys. Rev. B**65** (2002) 024405.

[9] Lin, J. Y. Y.; Kriplani, U.; Regehr, M.W.; Fultz, B.: Polarization factors for ^{57}Fe Mössbauer diffractions from polycrystals. Hyperfine Interact. **136** (2001) 663–672.

[10] Lin, J. Y. Y.; Fultz, B.: Site-specific long-range order in ^{57}Fe$_3$Al measured by Mössbauer diffractometry. Philos. Mag. **83** (2003) 2621–2640.

[11] Anthony, L.; Fultz, B.: Kinetic paths of B2 and DO$_3$ order parameters – theory. J. Mater. Res. **4** (1989) 1132–1139.

[12] Anthony, L.; Fultz, B.: Kinetics of B2, DO$_3$, and B32 ordering – results from pair approximation calculations and Monte-Carlo simulations. J. Mater. Res. **9** (1994) 348–356.

[13] Gao, Z. Q.; Fultz, B.: Transient B32-like order during the early stages of ordering in undercooled Fe$_3$Al. Philos. Mag. B**67** (1993) 787–800.

[14] Becker, M.; Schweika, W.: B32 order in iron rich Fe–Al alloys. Scripta Materialia **35** (1996) 1259.

[15] Stearns, M. B.: Spin-density oscillations in ferromagnetic alloys. I. localized solute atoms – Al Si Mn V and Cr in Fe. Phys. Rev. **147** (1966) 439–453.

[16] Frackowiak, J. E.: Determination of the long-range order parameter in the transition-metal alloys using Mössbauer-spectroscopy. Phys. Stat. Sol. **87** (1985) 109–119.

[17] Fultz, B.; Gao, Z. Q.: A Mössbauer spectrometry study of hyperfine magnetic-fields and ordering in Fe$_3$Al. Nucl. Instr. Meth. In Phys. Res. B**76** (1993) 115–120.

[18] Kriplani, U.: Kinematical Mössbauer Diffraction in ^{57}Fe. PhD thesis, California Institute of Technology, 2000.

[19] Fultz, B.: Suppressed kinetics of short-range ordering at low temperatures. J. Chem. Phys. **87** (1987) 1604–1609.

[20] Ouyang, H.; Fultz, B.: Percolation in alloys with thermally activated diffusion. J. Appl. Phys. **66** (1989) 4752–4755.

[21] Marcinkowski, M. J.; Brown, N.: Direct observation of antiphase boundaries in Fe$_3$Al superlattice. J. Appl. Phys. **33** (1962) 537.